Quasinormal modes of naked singularities in presence of nonlinear scalar fields

O. S. Stashko,[1,2] O. V. Savchuk,[3,4] and V. I. Zhdanov[5,6]

[1]Princeton University, Princeton, New Jersey 08544, USA
[2]Goethe Universität, Max-von-Laue Str. 1, Frankfurt am Main, 60438, Germany
[3]Facility for Rare Isotope Beams, Michigan State University, East Lansing, Michigan 48824, USA
[4]Bogolyubov Institute for Theoretical Physics, 03680 Kyiv, Ukraine
[5]Taras Shevchenko National University of Kyiv, Kyiv 01601, Ukraine
[6]Igor Sikorsky Kyiv Polytechnic Institute, Kyiv 03056, Ukraine

(Received 13 July 2023; accepted 4 December 2023; published 9 January 2024)

We study linear perturbations against static spherically symmetric background configurations of general relativity with a real scalar field (SF), which is minimally coupled with gravity; it is nonlinear due to the presence of the self-action potential. The background solutions have a naked singularity at the center of the configuration. The focus is on the stability of the background and fundamental frequencies of the quasinormal modes (QNM) of the axial perturbations in the Regge-Wheeler gauge. The problem is reduced to one hyperbolic master equation with an effective potential W_{eff}, which turns out to be positive for a general non-negative SF potential; this ensures the linear stability with respect to this kind of perturbations. For numerical simulations, the SF potential was chosen in the power-law form $V(\phi) \sim \phi^{2n}$ with $2 < n \leq 40$. We extracted the fundamental frequencies of QNM for different n and various sets of the background configuration parameters. The results show that even for a small background SF, there is a significant difference between the fundamental frequencies and ones in case of the Schwarzschild background. The results are also compared with the case of the Fisher-Janis-Newman-Winicour background dealing with a massless linear scalar field.

DOI: 10.1103/PhysRevD.109.024012

I. INTRODUCTION

Successful detections of gravitational waves [1,2] and the emerging prospects for multimessenger astronomy [3] have opened up new possibilities to test the gravitational theories in the strong field regime. This stimulated a surge of attention to damped oscillations of perturbed astrophysical objects as a source of gravitational radiation. These oscillations, known as quasinormal modes [4–7] carry important information about properties of relativistic objects, which, in particular, can be used, for example, to distinguish the black holes from the naked singularities arising in various gravitational theories. In this paper, we analyze theories with minimally coupled self-interacting scalar field (SF), which may be considered as simplest modifications of the general relativity. On the other hand, self-interacting SF is a workhorse of huge number of models dealing with the inflation of the Universe, dark energy etc.

If static spherically symmetric configuration contains only gravitational and scalar fields satisfying the conditions of asymptotic flatness, then the appearance of a naked singularity (NS) is expected in this system. An example is the well-known Fisher-Janis-Newman-Winicour (FJNW) solution [8–10]. The existence of NS has been demonstrated in case of a spherically symmetric static configuration with a fairly general SF potential [11,12]. Here we are faced with the main question: whether there are static configurations with SF and NS in our Universe at all. The no-hair theorems [13,14] say that the black hole with a regular nonzero SF cannot exist; so one can suppose that the scalar hair must simply dissipate during the collapse into the black hole. This would be in accordance with the cosmic censorship hypothesis [15]. On the other hand, there exist solutions in the general relativity and the other theories that describe NS (see, e.g., [16–20]), though, how they can be formed in our Universe is still a moot point. In this regard, it is appropriate to look for observational effects that can distinguish between normal black holes and their mimickers that contain NS.

The quasinormal modes (QNM) of the space-time vibrations emerging around relativistic objects can be good probes of different gravitational theories. Much attention has been paid to perturbations of the black holes and regular compact astrophysical objects (see, e.g., reviews [5–7]). QNM near NS have been studied in [21–25]; here, most works essentially deal with spherically symmetric background space-times, where an analytic representation of a background metric is available, such as in the Reissner-Nordstrom [21,23] and

FJNW [24] cases. Obviously, considerations of the linear perturbations are deeply connected with the stability analysis (see, e.g., [22,25,26] and references therein).

In the present paper, we study axial perturbations against the background formed by a isolated static spherically symmetric configuration of general relativity in presence of a minimally coupled nonlinear real SF. Our findings extend the results of [24], which deal with pure FJNW (massless linear case). In our case, the nonlinearity is introduced using a general SF-potential $V(\phi)$ satisfying the condition $\phi V'(\phi) \geq 0$, which grows more slowly than exponent for $|\phi| \to \infty$. In the numerical simulations we are dealing with the power-law SF potential.

In Sec. I the basic relations for static spherically symmetric background, are presented. In Sec. II we turn to numerical methods for the case of the power-law SF potential. We use the method of backward integration [11,27] to obtain the solutions of Einstein + SF equations for the background. In Sec. III we use the time-domain integration method [28] to solve the wave equations for the perturbations. Given these solutions, we use the Prony method [29] to extract the frequencies of the fundamental QNM. The final section summarizes the results.

II. ANALYTIC RELATIONS FOR GENERAL SF POTENTIAL

The action of standard general relativity in the presence of a minimally coupled real SF ϕ is given by[1]

$$S = \int d^4x\sqrt{-g}\left(-\frac{R}{16\pi G} + \frac{1}{2}\partial_\mu\phi\partial^\mu\phi - V(\phi)\right). \quad (1)$$

The background metric describes the static spherically symmetric space-time in Schwarzschild-like (curvature) coordinates:

$$ds^2 = e^{\alpha(r)}dt^2 - e^{\beta(r)}dr^2 - r^2d\Omega^2, \quad (2)$$

where $d\Omega^2 = d\theta^2 + (\sin\theta)^2 d\varphi^2$ and the radial variable $r > 0$.

In static spherically symmetric case we deal with two independent first-order Einstein equations

$$\frac{d}{dr}[r(e^{-\beta} - 1)] = -8\pi r^2[e^{-\beta}\phi'^2/2 + V(\phi)], \quad (3)$$

$$re^{-\beta}\frac{d\alpha}{dr} + e^{-\beta} - 1 = 8\pi r^2[e^{-\beta}\phi'^2/2 - V(\phi)], \quad (4)$$

and one second order equation for SF $\phi = \phi(r)$

$$\frac{d}{dr}\left[r^2 e^{\frac{\alpha-\beta}{2}}\frac{d\phi}{dr}\right] = r^2 e^{\frac{\alpha+\beta}{2}}V'(\phi). \quad (5)$$

Equations (3), (4), (5) define the background solutions under appropriate asymptotic conditions.

A small perturbation of the background solution will be considered in the linear approximation. The space-time metric and SF is then:

$$g_{\mu\nu} = g^{(0)}_{\mu\nu} + h_{\mu\nu}, \qquad \phi(x^\mu) = \phi_0(r) + \delta\phi(x^\mu), \quad (6)$$

where $g^{(0)}_{\mu\nu}$ and $\phi_0(r)$ represent the static spherically symmetric solution of (3)–(5), while $h_{\mu\nu} = h_{\mu\nu}(x^\mu)$ and $\delta\phi(x^\mu)$ represent the perturbations. There is extensive literature on the gravitational perturbations against spherically symmetric background (see, e.g., [6,30]).

The perturbation can be separated into axial and polar parts,[2] which can be treated independently. In this paper, we focus solely on the axial perturbations. The metrics of the axial gravitational perturbations $h_{\mu\nu}$ in the Regge-Wheeler gauge [31] take the following form

$$h^{\text{axial}}_{\mu\nu} = \begin{bmatrix} 0 & 0 & 0 & h_0(t,r) \\ 0 & 0 & 0 & h_1(t,r) \\ 0 & 0 & 0 & 0 \\ h_0(t,r) & h_1(t,r) & 0 & 0 \end{bmatrix} \left(\sin\theta\frac{\partial}{\partial\theta}\right) \times P_l(\cos\theta), \quad (7)$$

where $h_0(t,r)$ and $h_1(t,r)$ are two unknown functions, and $P_l(x)$ is the Legendre polynomial[3] with $l \geq 2$. After substitution of (7) to the Einstein-SF equations and retaining only linear terms, we obtain:

$$-h_0'(\alpha' + \beta') + 2h_0'' - h_0\left(\frac{2l(l+1)}{r^2}e^{\beta} + 2\alpha'' - \alpha'\beta' + \alpha'^2\right) + \dot{h}_1\left(\alpha' + \beta' - \frac{4}{r}\right) - 2\dot{h}_1' = 0, \quad (8)$$

$$\dot{h}_0' - \frac{2}{r}\dot{h}_0 - \ddot{h}_1 - \frac{l(l+1)-2}{r^2}e^{\alpha}h_1 = 0, \quad (9)$$

$$2h_1' + h_1(\alpha' - \beta') - 2e^{\beta-\alpha}\dot{h}_0 = 0. \quad (10)$$

[1]Units: $c = 1$; the metric signature is $(+---)$, $R^{\alpha}{}_{\beta\gamma\delta} = -R^{\alpha}{}_{\beta\delta\gamma} = \partial_\gamma\Gamma^{\alpha}_{\beta\delta} - \cdots$; $R_{\mu\nu} = R^{\alpha}{}_{\mu\alpha\nu}$. Below we rescale units of mass, length and SF so as to put $G = 1$ and to remove a coupling constant in the SF potential.

[2]In this case "axial" and "polar" [6,30] corresponds to "odd" and "even" according to the initial paper [31].

[3]Due to the spherical symmetry of the background configuration, more general case that involves Y_{lm}, leads to the same master equation and the same QNM frequencies. The perturbations with $l = 1$ can be removed by gauge transformation [32].

Here α, β correspond to the background solution. In agreement with [33], the perturbed part of SF equals to zero

$$\delta\phi = 0. \tag{11}$$

Equation (8) is redundant, because for perturbations $\sim e^{-i\omega t}$ it can be obtained from (9), (10).

After substitution

$$h_1(t,r) = re^{(\beta-\alpha)/2}\Psi(t,r), \tag{12}$$

and introducing the "tortoise" coordinate r^*

$$\frac{dr^*}{dr} = e^{(\beta-\alpha)/2}, \qquad r^*(0) = 0, \tag{13}$$

we can combine (9), (10) into a single master equation

$$\left(\frac{\partial^2}{\partial t^2} - \frac{\partial^2}{\partial r^{*2}}\right)\Psi(t,r^*) + W_{\text{eff}}(r,l)\Psi(t,r^*) = 0, \tag{14}$$

where

$$W_{\text{eff}}(r,l) = e^{\alpha-\beta}\left(\frac{\beta'-\alpha'}{2r} + e^{\beta}\frac{(l-1)(l+2)}{r^2} + \frac{2}{r^2}\right), \tag{15}$$

will be referred to as the "wave potential."

Using Eqs. (3), (4), we can rewrite (15) as

$$\begin{aligned} W_{\text{eff}}(r^*) &\equiv W_{\text{eff}}(r,l) \\ &= e^{\alpha}\left[8\pi V(\phi_0(r)) + \frac{(l-1)(l+2)-1}{r^2}\right] \\ &\quad + \frac{3}{r^2}e^{\alpha-\beta}, \end{aligned} \tag{16}$$

where $r = r(r^*)$ is defined by (13).

Further we fix $l \geq 2$; then $\forall\, r$: $W_{\text{eff}}(r^*) > 0$ in case of an arbitrary non-negative SF potential. This leads to the absence of bound states and stability of solutions of Eq. (14).

Under the condition of convergence of the integrals involved and for

$$\begin{aligned} &\lim_{r^*\to 0+0}\left[\frac{\partial\Psi(t,r^*)}{\partial t}\frac{\partial\Psi(t,r^*)}{\partial r^*}\right] = 0 \quad \text{and} \\ &\lim_{r^*\to\infty}\left[\frac{\partial\Psi(t,r^*)}{\partial t}\frac{\partial\Psi(t,r^*)}{\partial r^*}\right] = 0, \end{aligned} \tag{17}$$

we have a conserved quantity

$$E(t,\Psi) = \int_0^\infty dr^*\left\{\left(\frac{\partial\Psi}{\partial t}\right)^2 + \left(\frac{\partial\Psi}{\partial r^*}\right)^2 + W_{\text{eff}}(r^*)\Psi^2\right\}. \tag{18}$$

So far, we have formally dealt with arbitrary $V(\phi)$. Now, we need more detailed information concerning the properties of the system near the singular center. To do so, we impose the conditions [11]

$$V(0) = 0, \quad \phi V'(\phi) \geq 0, \quad |V'(\phi)| \leq C\exp(\kappa|\phi|^p), \tag{19}$$

where C, κ, p are positive constants, and $p < 1$. Under the latter condition, the terms with $V(\phi)$ in (3), (4), (5) do not directly contribute into the first two orders of the asymptotic expansion of ϕ, α, β for $r \to 0$ yielding

$$\phi(r) = -\xi\ln\left(\frac{r}{r_g}\right) + \phi_0 + O(r^{\eta+1}), \tag{20}$$

$$\begin{aligned} \alpha(r) &= (\eta-1)\ln\left(\frac{r}{r_g}\right) + \alpha_0 + O(r^{\eta+1}), \\ \beta(r) &= (\eta+1)\ln\left(\frac{r}{r_g}\right) + \beta_0 + O(r^{\eta+1}), \end{aligned} \tag{21}$$

where $\eta = 4\pi\xi^2 > 0$, and the constants ξ, η, α_0, β_0, and ϕ_0, which depend on Q, M, n, have been used to substantiate the asymptotic of $W_{\text{eff}}(r^*)$ below. The numerical values can be determined for the explicit form of $V(\phi)$. Note that the conditions imposed on V are satisfied in case of the power-law potential considered below.

Taking into account (20), (21), we get asymptotic relations near the singularity $(r \to 0, l \geq 2)$

$$\begin{aligned} r^* &= \frac{r^2}{2r_g}e^{(\beta_0-\alpha_0)/2}[1 + O(r^{\eta+1})], \\ W_{\text{eff}}(r,l) &= \frac{3e^{\alpha_0-\beta_0}r_g^2}{r^4}[1 + O(r^{\eta})], \\ W_{\text{eff}}(r^*) &= \frac{3}{4r^{*2}}[1 + O(r^{*\eta/2})]. \end{aligned} \tag{22}$$

In the presence of a naked singularity the space-time is not globally hyperbolic and evolution governed by (14) may be nonunique. However, it was shown [34,35] (see also [26,36,37]) that we immediately can have a well-defined dynamic, if there is a unique self-adjoint extension A_E of the spatial part of the wave operator (14). Using this, one can specify the boundary conditions at the singularity. We shall show that this is just the case of Eq. (14).

Equation (14) can be written as

$$\frac{\partial^2\Psi}{\partial t^2} = -A\Psi, \quad A = -\frac{d^2}{dr^{*2}} + W_{\text{eff}}(r^*), \quad r^* \in (0,\infty). \tag{23}$$

Following [34,35], we consider a positive symmetric operator A defined on $C_0^\infty(0,\infty)$ functions (with a compact support). Then we consider a self-adjoint extension A_E to have a well-defined dynamics governed by (14) leading to boundary conditions corresponding to A_E [34,35]. To check the essential self-adjointness we can use the Weyl's limit point-limit circle theorem [38].

A continuous function $W_{\rm eff}(r^*)$, $r^* \in (0,\infty)$, is said to be in the in the limit point case at zero (or infinity) [38], if for some λ, equation

$$-\frac{d^2\Psi}{dr^{*2}} + W_{\rm eff}(r^*)\Psi = -\lambda^2\Psi, \tag{24}$$

has at least one solution near zero (or infinity), which is not square integrable.

Now we assume that $V(\phi(r(r^*)))$ in (16) decays faster than r^{*-3} for $r^* \to \infty$. Then

$$W_{\rm eff}(r^*) = \frac{l(l+1)}{r^{*2}}\left[1 + O\left(\frac{\ln r^*}{r^*}\right)\right]. \tag{25}$$

Note that this is fulfilled in the case of the power-law potential considered in the next section. Then we have asymptotic solutions to (24)

$$\Psi(r^*) \simeq \sqrt{r^*}(C_1 J_{l+\frac{1}{2}}(\lambda r^*) + C_2 Y_{l+\frac{1}{2}}(\lambda r^*)), \quad r^* \to \infty, \tag{26}$$

which obviously is not square-integrable if we choose λ with $\mathrm{Im}\lambda \neq 0$; i.e. $W_{\rm eff}(r^*)$ is in the limit point case at $r \to \infty$.

Also, near the singularity we have

$$\Psi(r^*) \simeq C_1 r^{*\frac{3}{2}} + C_2 r^{*-\frac{1}{2}}, \qquad r^* \to 0, \tag{27}$$

where the solution with $C_2 \neq 0$ is not square integrable. Thus $W_{\rm eff}(r^*)$ is in the limit point case for $r^* \to 0$ as well. According to the Weyl limit point—limit circle theorem [38] operator A defined is essentially self-adjoint on $C_0^\infty(0,\infty)$.

Now A can be extended to a domain S, where $S \subset L^2$ is a set of functions $f(r^*)$, such that (i) $f(0) = 0$, (ii) $|f(r^*)|$ and $|df/dr^*|$ decay fast enough as $r^* \to \infty$, so that the integral $\int_0^\infty (|f'(x)|^2 + W_{\rm eff}(x)|f(x)|^2)dx < \infty$. The condition at $x = 0$ is sufficient to extract the unique solution of (27) with $C_2 = 0$ and to justify the null Dirichlet boundary condition at the center used in the numerical scheme used in Sec. IV.

It should be emphasized that this result is valid for a wide class of self-interaction potentials, which satisfy (19), and of course, includes the power-law potentials.

III. POWER-LAW POTENTIAL

Scalar field self-interation in the form of the power-law potential is considered:

$$V(\phi) = V_0|\phi|^{2n}, \tag{28}$$

where $V_0 > 0$ and $n > 2$ (not necessarily an integer). The latter condition means that we restrict ourselves to the case of the massless SF with the Coulomb behavior at spatial infinity, which requires $n > 2$ [11,27]; otherwise the asymptotic condition for ϕ will be different. Because the solution $\phi(r)$ of (5) has no zeros [11], we can choose the sign by setting $\phi(r) > 0$. From now on the units are set to $G = c = 1$ and the constant V_0 can be ruled out by rescaling r and ϕ.

We are interested in isolated configurations with spatially flat asymptotics, which satisfy the conditions

$$\lim_{r\to\infty}[r(e^{\alpha}-1)] = \lim_{r\to\infty}[r(e^{-\beta}-1)] = -r_g,$$
$$\lim_{r\to\infty}[r\phi(r)] = Q, \tag{29}$$

where $r_g = 2M$ and $M > 0$ is the configuration mass, Q is the "scalar charge." The global and asymptotic properties of the solutions satisfying (29) have been studied in [11,27]. For fixed $n > 2$ the solution of system (3)–(5) is uniquely defined by parameters M and Q [27]. There exists the naked singularity at the center ($r = 0$); the asymptotic behavior of the functions $\alpha(r)$, $\beta(r)$ and $\phi(r)$ is (20), (21). We use the backward integration starting from a sufficiently large initial radius $r_{\rm in}$ to smaller r up to the origin. The "initial" conditions at $r_{\rm in}$ were specified using the asymptotic relations [11,27] for $r \to \infty, n > 2$ that can be inferred from (29):

$$e^{\alpha} = \left(1 - \frac{r_g}{r}\right)\left[1 + O\left(\frac{\mu(r)}{r^2}\right)\right],$$
$$e^{-\beta} = \left(1 - \frac{r_g}{r}\right)\left[1 + \frac{4\pi Q^2}{r^2} + O\left(\frac{\mu(r)}{r^2}\right)\right], \tag{30}$$

$$\phi(r) = \frac{Q}{r}\left[1 + \frac{r_g}{2r} + \frac{n|Q|^{2n-2}}{(n-2)(2n-3)r^{2n-4}} + O\left(\frac{\mu(r)}{r^2}\right)\right]. \tag{31}$$

where $\mu(r) = 1/r$ for $n \geq 3$ and $\mu(r) = 1/r^{2n-4}$ for $2 < n < 3$. This yields for $r \to \infty$

$$r^* = r + r_g \ln(r/r_g) + O\left(\frac{1}{r}\right),$$
$$W_{\rm eff}(r) = \frac{l(l+1)}{r^2} + O\left(\frac{1}{r^3}\right),$$
$$W_{\rm eff}(r^*) = \frac{l(l+1)}{r^{*2}}\left(1 + O\left(\frac{\ln r^*}{r^*}\right)\right). \tag{32}$$

In our numerical calculations we have considered $r_{\rm in} = 10^5$. Examples of the qualitative behavior of the solutions are shown in Fig. 1 for some values of Q. The scalar field $\phi(r)$ decreases monotonically for all possible values of M, Q, n. As for the metric coefficients, $e^{\alpha(r)}$ increases monotonically from zero, whereas $e^{\beta(r)}$ increases form zero to some maximum and then decreases to 1. For large Q the maximum of $e^{\beta(r)}$ is almost invisible, but for small $Q \to 0$ the maximum of e^{β} increases indefinitely.

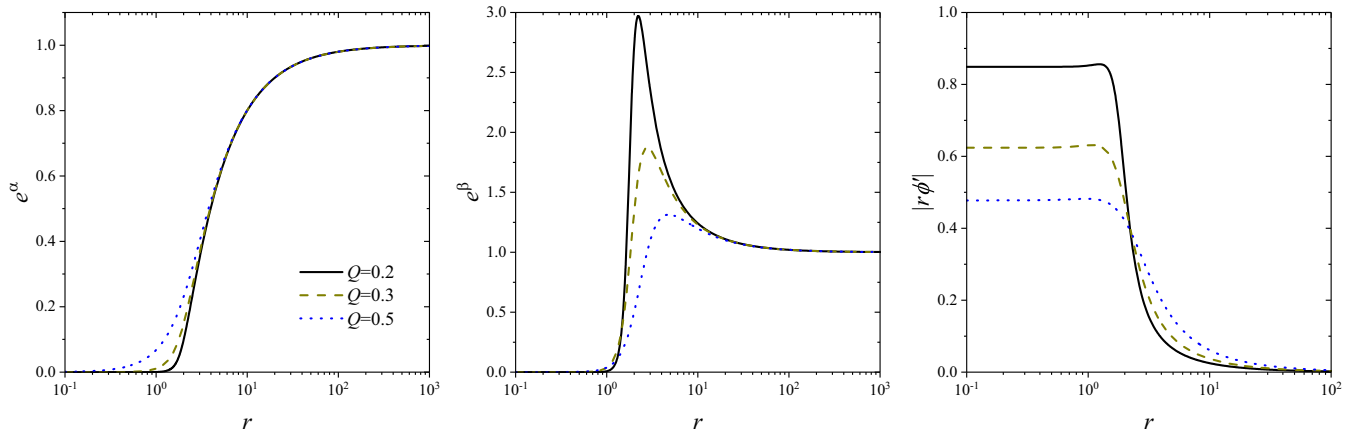

FIG. 1. Typical behavior of the background solutions of Einstein–SF equations. The examples are given for $M = 1$, $n = 3$ and (a) $Q = 0.5$; (b) $Q = 0.3$, (c) $Q = 0.2$. For smaller Q, the metric gets closer to the abscissa near the origin and approach the Schwarzschild values for $r > r_g$. Right panel shows how $|rd\phi/dr|$ tends to asymptotic value ξ of (20).

Also, for $Q \to 0$ the metric in the region $r > r_g$ tends to the Schwarzschild values, so all physical effects occurring in the this region will be indistinguishable from those of the Schwarzschild black hole. On the other hand, in the inner region ($r < r_g$), there is a cardinal difference from the Schwarzschild black hole even for small Q. This gives us a motivation to look for observational effects associated with the inner region, that may arise in the analysis of perturbations. The latter relation corresponds to (25).

IV. NUMERICAL SOLUTIONS TO THE MASTER EQUATION AND FREQUENCIES OF FUNDAMENTAL QNM

Our aim is to extract the fundamental QNM frequencies[4] of the axial space-time perturbations governed by (14). To do this, we solve this equation keeping in mind that the QNM frequencies reflect the internal properties of the background configuration; they do not depend on the form of the initial perturbation, which can be chosen with a large degree of arbitrariness.

The background configuration manifests itself by means of the wave potential in (14), which depends on the configuration parameters. Typical behavior of W_{eff} is shown in Fig. 2 for different Q, M and n, in panels (a), (b), (c), respectively. For a certain set of parameters, the effective potential can have a local maximum, which can disappears with increasing Q or decreasing M.

In order to integrate the master equation (14) and analyze the QNMs spectrum we use the time-domain integration method [7].

It is convenient to rewrite the wave equation (14) in terms of the null coordinates $u = t - r^*$, $v = t + r^*$:

$$4\frac{\partial^2}{\partial u \partial v}\Psi(u,v) + W_{\text{eff}}(u,v,l)\Psi(u,v) = 0. \tag{33}$$

Taking into account the remarks at the end of Sec. II in connection with asymptotic relations (22), following [34], we impose the null Dirichlet condition at $r^* = 0$:

$$\Psi(u = v, v) = 0. \tag{34}$$

Assuming that the ringtone frequencies are not sensitive to the form of the initial perturbation we chose a condition on characteristic $u = 0$ corresponding to the Gaussian wave packet:

$$\Psi(u = 0, v) = \exp\left[-\frac{(v - v_c)^2}{2\sigma^2}\right], \tag{35}$$

centered at $v = v_c = 50$, the width $\sigma = 1$.

To obtain numerical solutions, we use a second-order discretization scheme proposed by Chirenti and Rezzolla [28].

$$\Psi_N = (\Psi_W + \Psi_E)\frac{16 - \Delta^2 W_{\text{eff}}(S)}{16 + \Delta^2 W_{\text{eff}}(S)} - \Psi_S + O(\Delta^4), \tag{36}$$

where the indices (N, W, E, S) correspond to the points of the space-time triangular grid and as follows: $N = (u + \Delta, v + \Delta)$, $W = (u + \Delta, v)$, $E = (u, v + \Delta)$, $S = (u, v)$; Δ is the spacing between the grid points.

To extract fundamental frequencies $\omega = \omega_R + i\omega_I$, we fitted the time-domain profiles for a sufficiently large times and fixed r^* by a sum of complex exponentials $\Psi(t) \simeq \sum_{j=1}^{p} A_j e^{-i\omega_j t}$ using the Prony method [29].

Some typical examples of numerical solutions of (33) are presented on Fig. 3. The left panel (a) of this figure shows situation with small Q, when there is a series of echoes. The ringdown profile of damped QNM can be retrieved at a later

[4]Here the fundamental ω is that of QNM with the least damping, that is with the minimal value $\omega_I = \text{Im}(\omega)$.

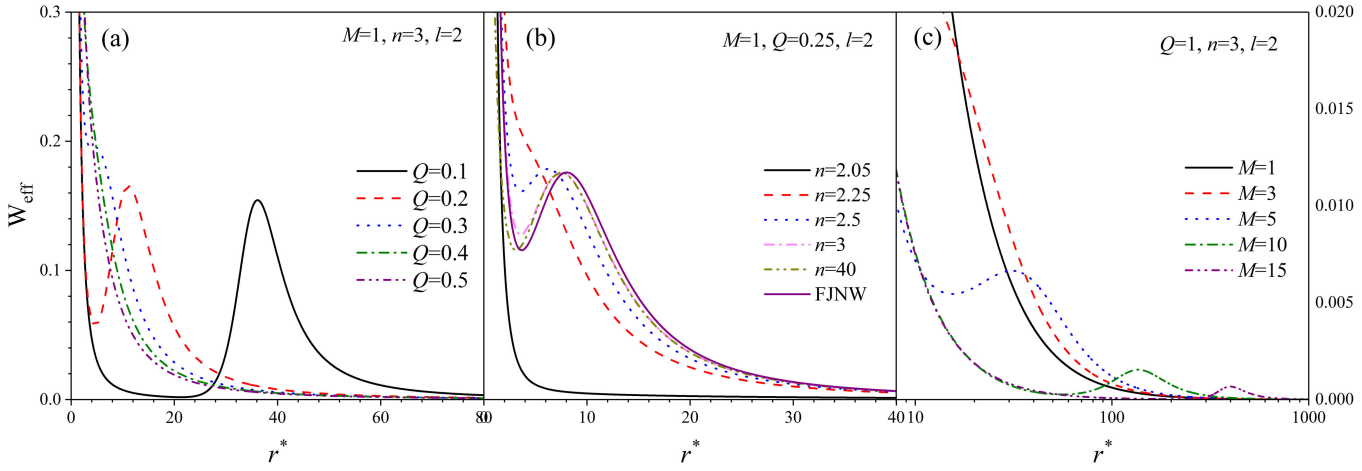

FIG. 2. Typical behavior of the effective potential $W_{\text{eff}}(r, l = 2)$: (a) $M = 1$, $n = 3$ for different Q; (b) $Q = 0.25$, $M = 1$, different n; (c) $Q = 1$, $n = 3$, different M.

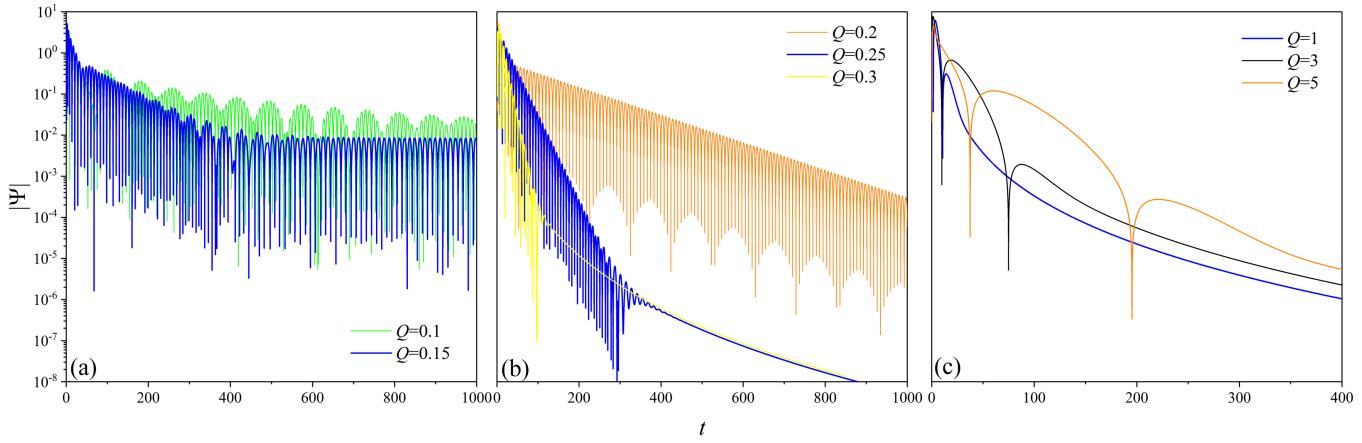

FIG. 3. Typical behavior of $|\Psi(t, r^* = 200)|$ for $l = 2$, $n = 3$, $M = 1$. The left panel shows QNM signal with echo noise due to the existence of the potential peak. For $Q = 0.15$ (blue graph) the echo dominates for $t \lesssim 500$; then the ringdown dominates. The blue and yellow curves on panel (b) show, how after the ringdown time we have typical power-law tails. The panel (c) also illustrates that for larger values of Q, the values of ω_R and ω_I becomes smaller and then, after finishing oscillations we have power-law tails.

time when the echo contribution is negligible. The series of the ringdown oscillations is followed by a power-law damping.

The derived fundamental QNM frequencies are presented in Tables I–II. We plotted the trajectories of these frequencies in the complex ω-plane as functions of one of the parameters M, Q, n with other parameters fixed (Figs. 5–8). As can be seen from Figs. 4 and 5, for smaller Q the fundamental frequencies get closer the FJNW values for all fixed n and M. Analogously, Figs. 6, 7 show how ω tend to the FJNW value as M grows.

As n grows, it seems that the fundamental frequencies approach FJNW ones (see Fig. 8). However, for large n we found a small feature shown in the inserts in Fig. 8. To be sure that this is not an artefact of calculations, we have checked the occurrence of analogous features for different choices of the parameters. We explain these features by an influence of the region near the singularity. In fact, the QNM are formed mainly far from the center; in this region, for large n the wave potential (14) is almost zero, as in the FJNW case. On the other hand, the effect of the region where $|\phi(r)| > 1$, becomes more tangible as n grows, but it is suppressed due to the null boundary condition (34); that is why these features are almost imperceptible.

V. DISCUSSION

We have studied axial linear perturbations against static spherically symmetric asymptotically flat background described by the Einstein–SF equations with the power-law SF potential. The background solutions necessarily have NS at the origin. The characteristic behavior of the perturbations induced by an initial pulse, has three main stages: (i) possible domination of echo signals, (ii) the ringdown stage followed by (iii) monotonous decay. The role and duration of these stages differ depending

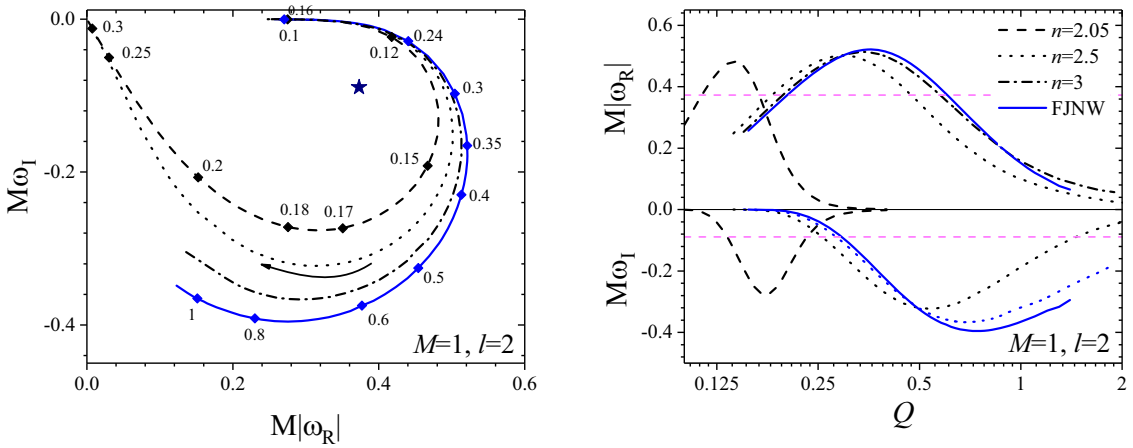

FIG. 4. Fundamental frequencies ω as functions of Q for three n values (indicated in the upper right corner of the right panel); $M = 1$, $l = 2$. Solid blue curves correspond to the FJNW case. Left panel: trajectories $\omega(Q)$ in the complex plane; black arrow shows the direction of increasing Q and the numbers near corresponding points of the dashed and solid blue curves indicate the values of Q; the blue star shows the Schwarzschild case. Right panel shows separately $\omega_R(Q)$ and $\omega_I(Q)$; the horizontal dashed lines correspond to the Schwarzschild case.

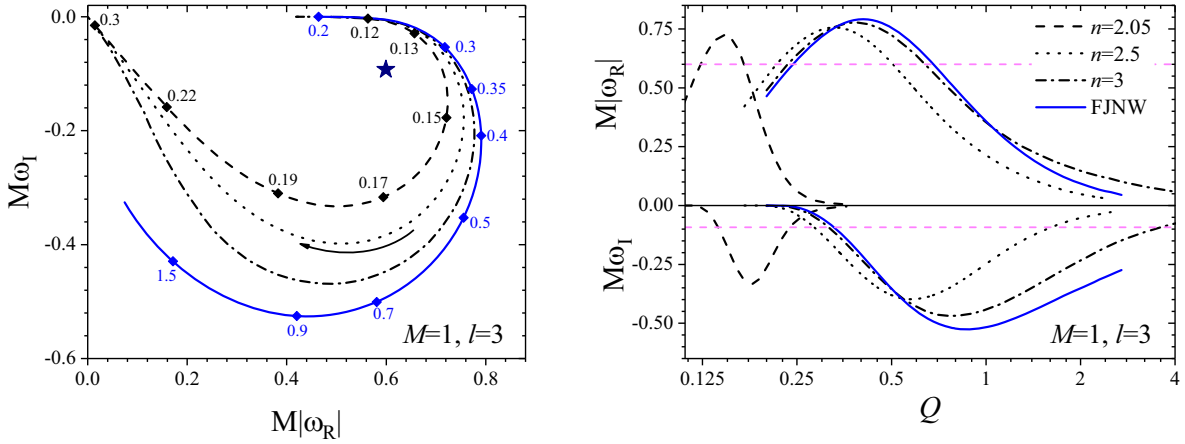

FIG. 5. The same as on Fig. 4 for $M = 1$, $l = 3$.

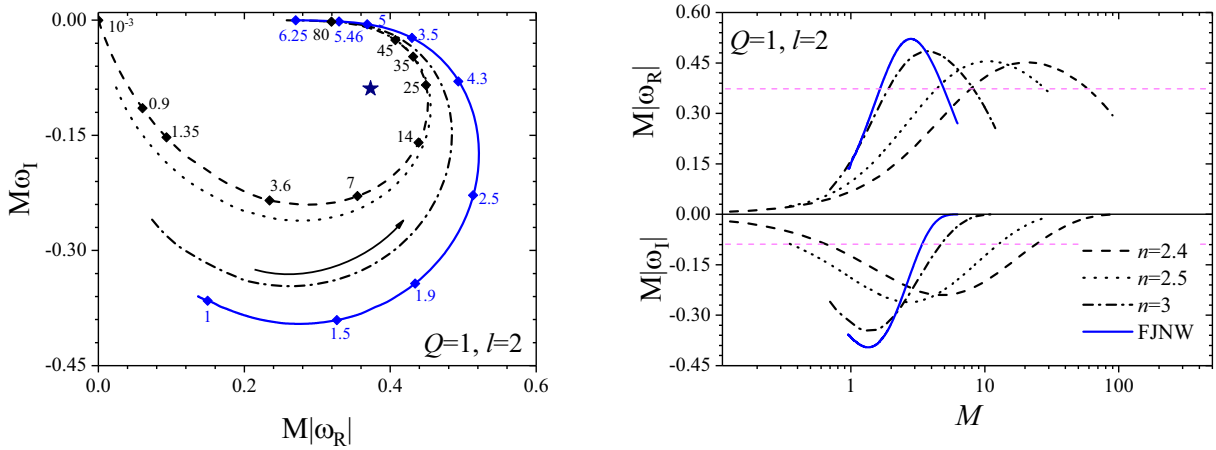

FIG. 6. Fundamental frequencies ω as functions of M for different n values (indicated in the right lower corner of the right panel); $l = 2$, $Q = 1$. Left panel: trajectories $\omega(M)$ in the complex plane; black arrow shows the direction of increasing M and the numbers near the corresponding points of the dashed and solid blue curves indicate the values of M; the blue star shows the Schwarzschild case. Right panel shows separately dependencies $\omega_R(M)$ and $\omega_I(M)$; the horizontal dashed lines correspond to the Schwarzschild case.

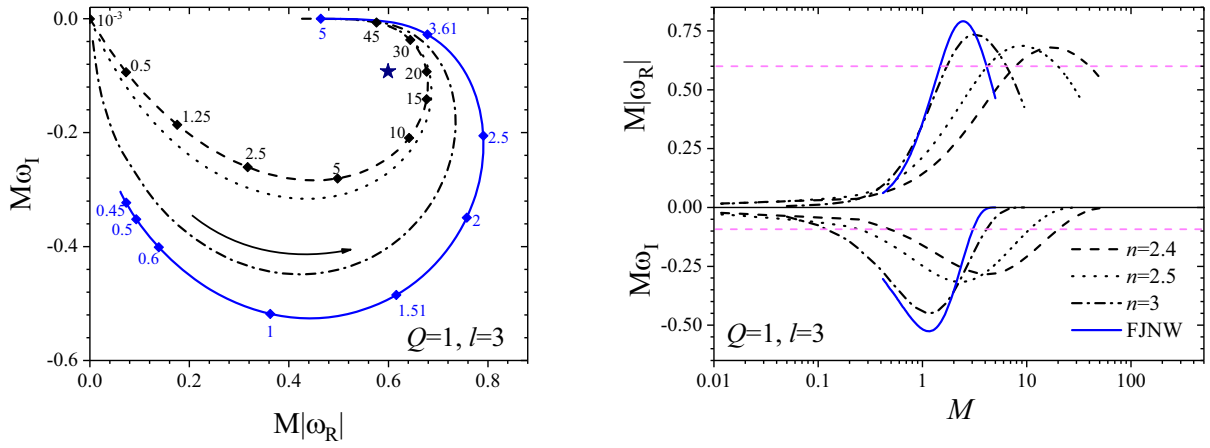

FIG. 7. The same as on Fig. 6 for $Q = 1$, $l = 3$.

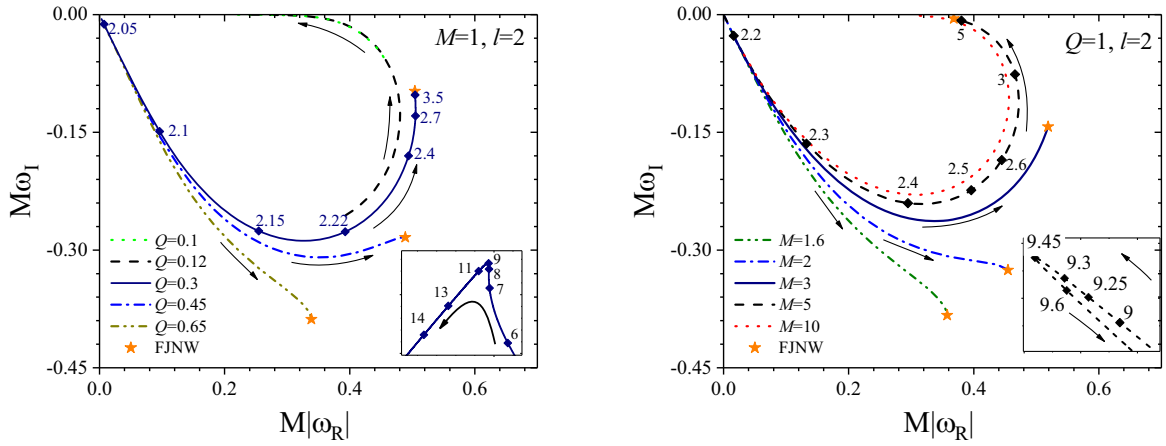

FIG. 8. The fundamental frequencies ω in the complex plane $\omega_R \times \omega_I$ as functions of n for $l = 2$. Left panel: trajectories $\omega(n)$ for fixed $M = 1$ and several different Q; the numbers near the corresponding points of some curves indicate the values of n. Right panel: the same for $Q = 1$ and several different M. Black arrows show the direction of increasing n. As n increases, $\omega(n)$ approach FJNW values (orange stars); however, for sufficiently large n we found typical small features shown in the insets.

on the configuration parameters affecting the wave potential (16); for example, sometimes the stage (i) may be substantially absent. We were mostly interested in stage (ii) of the QNM domination yielding the fundamental frequencies of these modes. The results of the numerical simulations are presented in Tables I and II; they are used in Figs. 4–8 for different sets of the background configuration parameters.

We also draw attention to the analytic result described by Eqs. (14), (16) that have been used for the general SF potential $V(\phi) \geq 0$ to study stability issues. In particular, we used this in case of the rather general $V(\phi)$, when the background solutions have an appropriate asymptotic near the naked singularity. Of course, this does not yet solve the entire problem of the stability of the NS, since we have limited ourselves to axial perturbations. The polar perturbations deserve a separate study and we plan to consider this issue elsewhere.

The presence of the nonzero SF potential manifests itself in the values ω of the fundamental QNM frequencies that are different for different background configuration parameters. There is also a considerable difference from the FJNW values. However, the qualitative behavior of trajectories in the ω-plane is rather similar to the FJNW curves. For fixed M, the ω-trajectories get closer to the FJNW curves in the intervals of smaller Q (Figs. 4–5). Therefore, for smaller SF the influence of the power-law potential decreases. A similar trend is also observed for a fixed Q, when M gets larger (Figs. 6–7). For large n, the wave potential and ω-trajectories can be well approximated by the FJNW curves; nevertheless the nonlinear effects manifest themselves though the small features that are almost imperceptible. On the whole, the FJNW case satisfactory describes the qualitative behavior of ω-trajectories. Of course, this cannot be said about the numerical values of the fundamental QNM frequencies.

If SF is small enough, its influence in the outer region ($r > r_g$) is becomes negligible. In particular, this concerns the effects in motion of particles and photons, structure of accretion disks etc. On the other hand, it is important to note that in the region $r < r_g$, the significant differences from the Schwarzschild case persist even for small Q. This can be explained by different boundary conditions: the Dirichlet condition at the naked singularity in presence of SF versus the in-going wave condition at the black hole horizon in the Schwarzschild case. The boundary condition at the origin feels the difference of NS from the black hole even when SF is arbitrarily small. Thus, the fundamental frequencies of the configuration considered, differ qualitatively and numerically from those in case of the Schwarzschild solution even for a small scalar field. One can suggest that this is a fairly general property of static systems with the scalar field leading to the occurrence of naked singularity.

ACKNOWLEDGMENTS

We are indebted to Prof. Luciano Rezzolla for helpful discussions. The work of V. I. Z. was supported by the National Research Foundation of Ukraine under Project No. 2020.02/0073. O. S. is grateful to Igor Klebanov and Horst Stoecker for their kind hospitality.

APPENDIX: TABLES

TABLE I. The fundamental quasinormal mode $M\omega$ of the NS with nonlinear SF [$M = 1$, $n = (2.1, 3)$] and FJNW for various values of Q. The first line corresponds to the Schwarzschild black hole.

	$n = 2.1$		$n = 3$		FJNW	
Q	$l = 2$	$l = 3$	$l = 2$	$l = 3$	$l = 2$	$l = 3$
0	$0.3730 - 0.0891i$	$0.5993 - 0.0927i$	$0.3730 - 0.0891i$	$0.5993 - 0.0927i$	$0.3730 - 0.0891i$	$0.5993 - 0.0927i$
0.2	$0.4303 - 0.2425i$	$0.6917 - 0.2536i$	$0.3815 - 0.0077i$	$0.489 - 0.0002i$	$0.3683 - 0.0052i$	$0.4643 - 0.00009i$
0.25	$0.2172 - 0.2558i$	$0.4005 - 0.322i$	$0.4639 - 0.048i$	$0.6413 - 0.01445i$	$0.45481 - 0.0381i$	$0.6196 - 0.0084i$
0.3	$0.0874 - 0.1371i$	$0.1731 - 0.1748i$	$0.5051 - 0.112i$	$0.7293 - 0.0701i$	$0.5042 - 0.09739i$	$0.7179 - 0.0534i$
0.35	$0.0346 - 0.0573i$	$0.0692 - 0.0712i$	$0.5131 - 0.1799i$	$0.7703 - 0.1484i$	$0.5214 - 0.166i$	$0.7723 - 0.1268i$
0.45	$0.0066 - 0.0112i$	$0.01323 - 0.0137i$	$0.4682 - 0.2874i$	$0.7567 - 0.2992i$	$0.4888 - 0.2839i$	$0.7824 - 0.286i$
0.55	$0.00194 - 0.0034i$	$0.0039 - 0.0041i$	$0.3933 - 0.3449i$	$0.6803 - 0.3998i$	$0.4161 - 0.3558i$	$0.7172 - 0.4067i$
0.65	$0.00081 - 0.0014i$	$0.0016 - 0.0017i$	$0.3203 - 0.3653i$	$0.5898 - 0.4512i$	$0.3388 - 0.388i$	$0.6269 - 0.4791i$

TABLE II. The fundamental quasinormal mode $M\omega$ of the NS with nonlinear SF [$M = 1$, $Q = (0.15, 0.3, 0.45)$] and FJNW for various values of n. The first and second lines correspond to the Schwarzschild black hole and FJNW solutions, respectively.

	$Q = 0.15$		$Q = 0.3$		$Q = 0.45$	
n	$l = 2$	$l = 3$	$l = 2$	$l = 3$	$l = 2$	$l = 3$
Schw	$0.3730 - 0.0891i$	$0.5993 - 0.0927i$	$0.3730 - 0.0891i$	$0.5993 - 0.0927i$	$0.3730 - 0.0891i$	$0.5993 - 0.0927i$
FJNW	$0.2436 - 0.00006i$	$0.2796 - 6 \times 10^{-8}i$	$0.5042 - 0.0974i$	$0.7183 - 0.0535i$	$0.4888 - 0.2839i$	$0.7824 - 0.286i$
2.05	$0.467 - 0.1918i$	$0.721 - 0.1773i$	$0.0073 - 0.0123i$	$0.0146 - 0.0151i$	$0.0006 - 0.001i$	$0.0012 - 0.0013i$
2.1	$0.4517 - 0.0484i$	$0.6305 - 0.0158i$	$0.0876 - 0.1369i$	$0.173 - 0.1748i$	$0.0066 - 0.0112i$	$0.01324 - 0.0137i$
2.3	$0.3178 - 0.0012i$	$0.3861 - 6 \times 10^{-6}i$	$0.4698 - 0.2222i$	$0.7352 - 0.2153i$	$0.2654 - 0.2943i$	$0.4839 - 0.3661i$
2.5	$0.2802 - 0.00029i$	$0.33 - 6 \times 10^{-7}i$	$0.5016 - 0.1558i$	$0.7475 - 0.1226i$	$0.3952 - 0.306i$	$0.6675 - 0.3476i$
3	$0.2532 - 0.00009i$	⋯	$0.5052 - 0.112i$	$0.7293 - 0.0701i$	$0.4682 - 0.2874i$	$0.7567 - 0.2992i$
4	$0.245 - 0.00007i$	⋯	$0.5044 - 0.0995i$	$0.7201 - 0.056i$	$0.4867 - 0.2837i$	$0.7793 - 0.2869i$
5	$0.2439 - 0.0000633i$	⋯	$0.50427 - 0.0979i$	$0.7188 - 0.0541i$	$0.4885 - 0.2839i$	$0.7819 - 0.2862i$
7	$0.2436 - 0.0000625i$	⋯	$0.50426 - 0.0976i$	$0.7184 - 0.0536i$	$0.48882 - 0.28394i$	$0.7824 - 0.2861i$
10	$0.2436 - 0.0000624i$	⋯	$0.50426 - 0.0975i$	$0.7184 - 0.0535i$	$0.48886 - 0.28395i$	$0.7825 - 0.2861i$

[1] LIGO Scientific and Virgo Collaborations, Phys. Rev. Lett. **116**, 061102 (2016).
[2] LIGO Scientific and Virgo Collaborations, arXiv:2108.01045.
[3] S. Ronchini, M. Branchesi, G. Oganesyan, B. Banerjee, U. Dupletsa, G. Ghirlanda, J. Harms, M. Mapelli, and F. Santoliquido, Astron. Astrophys. **665**, A97 (2022).
[4] H.-P. Nollert, Classical Quantum Gravity **16**, R159 (1999).
[5] K. D. Kokkotas and B. G. Schmidt, Living Rev. Relativity **2**, 2 (1999).
[6] E. Berti, V. Cardoso, and A. O. Starinets, Classical Quantum Gravity **26**, 163001 (2009).
[7] R. A. Konoplya and A. Zhidenko, Rev. Mod. Phys. **83**, 793 (2011).
[8] I. Z. Fisher, Zh. Exp. Theor. Phys. **18**, 636 (1948).
[9] A. I. Janis, E. T. Newman, and J. Winicour, Phys. Rev. Lett. **20**, 878 (1968).
[10] K. S. Virbhadra, Int. J. Mod. Phys. A **12**, 4831 (1997).
[11] V. I. Zhdanov and O. S. Stashko, Phys. Rev. D **101**, 064064 (2020).
[12] O. Stashko and V. I. Zhdanov, Galaxies **9**, 72 (2021).
[13] J. D. Bekenstein, Phys. Rev. Lett. **28**, 452 (1972).
[14] J. D. Bekenstein, Phys. Rev. D **5**, 1239 (1972).
[15] R. Penrose, Phys. Rev. Lett. **14**, 57 (1965).
[16] D. Christodoulou, Commun. Math. Phys. **93**, 171 (1984).
[17] A. Ori and T. Piran, Phys. Rev. Lett. **59**, 2137 (1987).
[18] P. S. Joshi and I. H. Dwivedi, Phys. Rev. D **47**, 5357 (1993).
[19] P. S. Joshi, D. Malafarina, and R. Narayan, Classical Quantum Gravity **31**, 015002 (2013).
[20] Y. C. Ong, Int. J. Mod. Phys. A **35**, 2030007 (2020).
[21] C. Chirenti, A. Saa, and J. Skákala, Phys. Rev. D **86**, 124008 (2012).
[22] B. Khamesra and V. Suneeta, Phys. Rev. D **90**, 024044 (2014).
[23] E. C. Santos, J. C. Fabris, and J. A. de Freitas Pacheco, arXiv:1903.04874.
[24] A. Chowdhury and N. Banerjee, Phys. Rev. D **102**, 124051 (2020).
[25] A. Chowdhury, S. Devi, and S. Chakrabarti, Phys. Rev. D **106**, 024023 (2022).
[26] G. Dotti, Universe **8**, 38 (2022).
[27] O. S. Stashko, V. I. Zhdanov, and A. N. Alexandrov, Phys. Rev. D **104**, 104055 (2021).
[28] C. B. M. H. Chirenti and L. Rezzolla, Classical Quantum Gravity **24**, 4191 (2007).
[29] E. Berti, V. Cardoso, J. A. González, and U. Sperhake, Phys. Rev. D **75**, 124017 (2007).
[30] S. Chandrasekhar, *The Mathematical Theory of Black Holes* (Clarendon Press, 1998).
[31] T. Regge and J. A. Wheeler, Phys. Rev. **108**, 1063 (1957).
[32] C. V. Vishveshwara, Phys. Rev. D **1**, 2870 (1970).
[33] T. Kobayashi, H. Motohashi, and T. Suyama, Phys. Rev. D **85**, 084025 (2012).
[34] R. M. Wald, J. Math. Phys. (N.Y.) **21**, 2802 (1980).
[35] A. Ishibashi and R. M. Wald, Classical Quantum Gravity **20**, 3815 (2003).
[36] A. Ishibashi and A. Hosoya, Phys. Rev. D **60**, 104028 (1999).
[37] G. W. Gibbons, S. A. Hartnoll, and A. Ishibashi, Prog. Theor. Phys. **113**, 963 (2005).
[38] M. Reed and B. Simon, *Methods of Modern Mathematical Physics. 2. Fourier Analysis, Self-Adjointness* (Academic Press, New York, 1975), Vol. 2.